ASTRONOMY
AND
ASTROPHYSICS

Beaming and precession in the inner jet of 3C 273

II. The central engine

G.E. Romero[1],[⋆], L. Chajet[2], Z. Abraham[3], and J.H. Fan[4]

[1] Instituto Argentino de Radioastronomía, C.C.5, (1894) Villa Elisa, Bs. As., Argentina
[2] Facultad de Ciencias Astronómicas y Geofísicas, UNLP, Paseo del Bosque, 1900 La Plata, Argentina
[3] Universidade de São Paulo, Instituto Astronômico e Geofísico, Av. M. Stefano 4200, CEP 04301-904 São Paulo, SP, Brazil
[4] Guangzhou Normal University, Center for Astrophysics, Guangzhou 510400, P.R. China

Abstract. The quasar 3C 273 is a well-known superluminal source. More than 10 radio components have been detected moving away from the nucleus with different superluminal speeds and position angles. The pattern of ejection suggests the existence of a precessing inner jet, whose kinematics has been discussed by Abraham & Romero (1999). We now present a binary black hole model for the central engine of 3C 273 where the rapid precession is tidally induced in the primary accretion disk inner region by a secondary black hole in a non-coplanar orbit. Using γ- and X-ray data we estimate upper limits for the mass of the primary, and then we compute the relevant parameters of the system for a variety of disk models. We also discuss some of the implications of the model for the electromagnetic and gravitational radiation from 3C 273.

Key words: galaxies: quasars: individual: 3C 273 – gamma rays: theory – black hole physics

1. Introduction

The bright radio source 3C 273 is one of the most extensively studied active galactic nucleus. It was first identified as a quasar at redshift $z = 0.158$ by Schmidt (1963). Detailed observations of this object have been performed during more than 35 years, including simultaneous measurements of its spectrum from radio to γ-ray energies (Lichti et al. 1995) and multiwavelengths variability studies for equally wide energy ranges (von Montigny et al. 1997).

3C 273 has been also subject to intense VLBI monitoring since Cohen et al. (1971) measured its superluminal expansion velocity. At least ten superluminal components have been detected moving away from the optically thick radio core (e.g. Unwin et al. 1985, Biretta et al. 1985, Cohen et al. 1987; Zensus et al. 1988, 1990; Krichbaum et al. 1990, Abraham et al. 1996). Additional short-lived components have been almost surely missed during the gaps between observations.

Recently, Abraham & Romero (1999, hereafter Paper I) have used all available VLBI data of superluminal components in 3C 273 to determine the kinematic evolution of the inner jet. They have shown that the different velocities and position angles at the ejection time of the various well-monitored components are consistent with the existence of a precessing inner jet in the quasar. Fits of the VLBI data suggest a period of precession of ~ 16 years in the observer's frame. For a Hubble constant parameter $h = 0.7$ ($H_0 = 100h$ km s^{-1} Mpc^{-1}), the jet would have a bulk Lorentz factor $\gamma \sim 10.8$ and precess within a cone of half-opening angle $\sim 3.9°$. The Doppler factor should vary between 2.8 and 9.4 due to the changing viewing angle. The implications of such an oscillation in the value of the Doppler factor for the observable emission along the electromagnetic spectrum of 3C 273 were explored in Paper I.

In this paper we present and discuss a supermassive binary black hole model which could explain the jet precession in 3C 273. We shall assume that the inner jet and the innermost parts of the accretion disk that surrounds the primary black hole are coupled in such a way that a precession of the disk induces a precession of the jet, as it is thought to occur in galactic binary systems like SS433 (e.g. Katz 1980). A secondary black hole in a close non-coplanar orbit can exert a tidal perturbation on the disk that can result in the near-rigid body precession of its innermost regions (e.g. Katz 1997). We shall use γ- and X-ray data, along with the information obtained from the VLBI radio observations, to constrain the black hole masses and other parameters of the system.

Supermassive black hole binaries (SBHBs) are the natural result of galaxy mergers. Their formation and evolution have been extensively discussed in the literature (e.g. Begelman et al. 1980, Roos 1981, Valtaoja et al. 1989). The fact that many (if not most) galaxies contain massive black holes and that galaxies often merge implies a relatively high formation rate of SBHBs. The current evidence for central engines of active galactic nuclei formed by massive binary systems includes double nuclei (as in the case of NGC4486B), wiggly jets (e.g. Kaastra & Roos 1992), double emission lines observed in several quasars (Gaskell 1996), and periodic optical light curves as in the case

---

Send offprint requests to: G.E. Romero (romero@irma.iar.unlp.edu.ar)
[⋆] Membern of CONICET

of OJ 287 (Sillanpää et al. 1988, Lehto & Valtonen 1996, Villata et al. 1998).

Geodetic precession of relativistic jets in SBHBs has also been often discussed in relation to large-scale helical jets (e.g. Begelman et al. 1980, Roos 1988). This effect is due to the Lense-Thirring dragging of inertial frames and is much slower than the tidal induced precession that will be studied here. The geodetic precession of the primary in SBHBs occurs with a period of $P_{\rm geod} \sim 9 \times 10^8 r^{5/2}(M/m)M_8^{-3/2}$ yr, where r is the black hole separation in pc, M_8 the mass of the primary in units of $10^8 \, M_\odot$, and M/m is the primary to secondary mass ratio. This kind of precession cannot be applied to stable sources with short periods ($\sim$ a few years) because gravitational losses rapidly become catastrophic.

Roos et al. (1993) have studied the small-scale wiggling jet of 1928+738 in the context of a binary black hole system, using a different approach: they have assumed that the jet complex structure is the result of the velocity modulation produced by the orbital motion of the hole that accelerates the jet in the supermassive binary.

In the case of 3C 273, where the existence of a prominent accretion disk around the primary can be inferred form the strong blue bump in the spectrum (e.g. Malkan 1983, Kriss et al. 1999), a tidally induced precession of the jet seems to be the more plausible explanation of the jet behaviour at VLBI scales. In the next sections we will discuss the details of this scenario.

2. Disk tidal perturbation

2.1. Framework

Let us consider a central black hole of mass M surrounded by an accretion disk with inner radius $r_{\rm in}$ and outer radius $r_{\rm out}$. Self-gravity is assumed to be negligible up to distances of $\sim$ few hundreds of $r_{\rm g}$ from the hole, where $r_{\rm g} = GM/c^2$ is the gravitational radius (Sakimoto & Coroniti 1981). Two relativistic jets are collimated perpendicularly to the disk near the central black hole and propagate in opposite directions. A secondary hole of mass m is in a circular non-coplanar orbit of radius $r_{\rm m}$ with an inclination angle θ to the plane of the disk. It is expected that the tidal interactions between the disk and the secondary result in the precession of the innermost part of the disk, where the communication among the different fluid elements can be sufficiently fast to allow a near-rigid body behaviour. This disk precession is transmitted to the jets, which also precess at the same rate within a cone of half-opening angle θ.

A sketch of the situation is presented in Fig. 1, where the orbital plane of the binary system is coincident with the xy-plane. Just one of the jets and the precessing part of the disk, whose outer radius is $r_{\rm d}$, are represented here. The disk Keplerian angular velocity is $\omega_{\rm d} = (GM/r_{\rm d}^3)^{1/2}$. The secondary orbital period is $T_{\rm m}$ and the associated angular velocity $\omega_{\rm m} = 2\pi/T_{\rm m}$.

Tidally induced precession of accretion disks in X-ray binaries and young stellar systems have been studied by several authors in the last 25 years (e.g. Katz 1973, 1980; Katz et al. 1982; Papaloizou & Terquem 1995; Larwood et al. 1996; Lar-
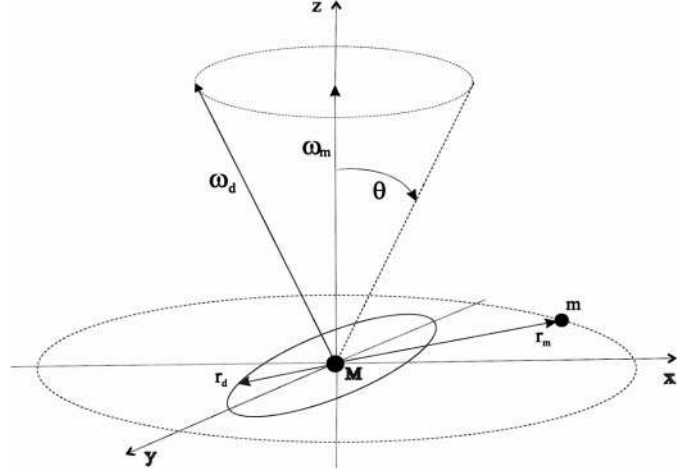

Fig. 1. A sketch (drawn not at scale) of the precessing disk model for 3C 273. Jet direction is indicated by $\boldsymbol{\omega}_{\rm d}$.

wood 1997, 1998; Terquem et al. 1999; Wijers & Pringle 1999). However, except by the paper by Katz (1997) on OJ 287, the application of tidally-driven precession to blazars remains mostly unexplored.[1]

2.2. Dynamics

The dynamics of the disk is determined by the equations of motion and continuity. They can be written as:

$$\frac{\partial \boldsymbol{v}}{\partial t} + (\boldsymbol{v}\boldsymbol{\nabla})\boldsymbol{v} = -\frac{1}{\rho}\boldsymbol{\nabla}P - \boldsymbol{\nabla}\Phi + \boldsymbol{f}_{\rm visc} \tag{1}$$

and

$$\frac{\partial \rho}{\partial t} + \boldsymbol{\nabla}(\rho\boldsymbol{v}) = 0, \tag{2}$$

where P denotes the pressure, ρ the density, $\boldsymbol{v}$ the velocity of the fluid, $\boldsymbol{f}_{\rm visc}$ the viscous force per unit of mass, and Φ is the external gravitational potential given by:

$$\begin{aligned} \Phi &= \Phi_{\rm M} + \Phi_{\rm m} \\ &= -\frac{GM}{r} - \frac{Gm}{|\boldsymbol{r} - \boldsymbol{r}_{\rm m}|} + \frac{Gm \, \boldsymbol{r}.\boldsymbol{r}_{\rm m}}{r_{\rm m}^3}. \end{aligned} \tag{3}$$

The first term in the second member of Eq. (3) is the potential due to the primary whereas the other two terms are the effect of the perturbing action of the secondary.

The equation of state is assumed to be polytropic:

$$P = K\rho^{1+1/n}, \tag{4}$$

where K and n are the polytropic constant and index, respectively. The sound speed is

$$c_{\rm s} = \sqrt{\frac{dP}{d\rho}} \sim H\omega_{\rm d}, \tag{5}$$

---

[1] See also the paper by Papaloizou et al. (1998), where the case of the moderately active galaxy NGC 4258 is discussed.

with H the disk half-thickness. The surface mass density is defined by

$$\Sigma = \int_{-H}^{+H} \rho \, dz. \tag{6}$$

2.3. Precession

If the perturbation is small then Eqs. (1) and (2) can be linearized. The perturbative potential can be decomposed into a linear sum of contributions corresponding to odd and even terms in z and written as (see Larwood 1997 for details):

$$
\begin{aligned}
\Phi_{\rm m} &= \Phi_{\rm e} + \Phi_{\rm o} \\
&= \frac{3}{4} \frac{Gm}{r_{\rm m}^3} r^2 \cos^2 \theta \exp(2i\phi) \\
&\quad + i \frac{3}{2} \frac{Gm}{r_{\rm m}^3} rz \sin^2 \theta \exp(i\phi)
\end{aligned} \tag{7}
$$

The term $\Phi_{\rm o}$ is responsible for the disk precession. The precession frequency $\Omega_{\rm p}$ can be calculated following Papaloizou & Terquem (1995) and Larwood (1997) by:

$$\Omega_{\rm p} \sin \theta = \frac{i}{2} \frac{\int \Sigma \frac{\partial \Phi_{\rm o}}{\partial z} r^2 \, dr}{\int \Sigma r^3 \omega_{\rm d} dr}, \tag{8}$$

which leads, integrating from $r = 0$ to $r = r_{\rm d}$ and assuming a constant Σ, to:

$$\Omega_{\rm p} = -\frac{3}{4} \left(\frac{7 - 2n}{5 - n} \right) \frac{Gm}{r_{\rm m}^3} \frac{r_{\rm d}^2}{(GMr_{\rm d})^{1/2}} \cos \theta. \tag{9}$$

For a gas with index $n = 1.5$, this is basically the same result obtained by Katz et al. (1982) in the case of a precessing ring:

$$\Omega_{\rm p} \approx -\frac{3}{4} \frac{Gm}{r_{\rm m}^3} \frac{1}{\omega_{\rm d}} \cos \theta. \tag{10}$$

In the case of 3C 273, the precession frequency in the source frame, inferred from the VLBI radio data, is (see Paper I) $\Omega_{\rm p} \approx 1.44 \times 10^{-8} \, {\rm s}^{-1}$, and the half-opening angle $\theta \sim 3.9°$ (throughout the paper we shall adopt a Hubble and deceleration parameters of $h = 0.7$ and $q_0 = 1/2$, respectively). We shall use the result of variability observations of 3C 273 at different wavelengths to obtain upper limits to the mass of the primary (which is responsible for the high energy emission) and secondary (which could produce optical periodic signals in the lightcurve) black holes in the system.

3. Mass of the primary

3.1. High energy emission from 3C 273

Gamma-rays from 3C 273 were first detected by the Cos B satellite in the 1970s (Swanenburg et al. 1978, Bignami et al. 1981). The EGRET instrument on board the Compton Observatory detected again high energy flux densities from this object in 1991 (von Montigny et al. 1993) and 1993 (von Montigny et al. 1997). In this latter opportunity the flux changed by a factor ~ 3 over a

timescale $t_{\rm v} = F_{\rm min}(\Delta F/\Delta t)^{-1} \sim 10^6$ s. Simultaneous measurements at X-ray energies were made with the ASCA satellite (von Montigny 1997).

Blazars like 3C 273 are compact γ-ray sources in the sense that they present X-ray radiation fields generated by the inner accretion disk regions that make the source opaque to γ-rays up to distances of the order of a few hundreds of gravitational radii (e.g. Becker & Kafatos 1995). The γ-rays are absorbed in the disk radiation field to produce electron-positron pairs in a cascade process (e.g. Blandford & Levinson 1995). When the source becomes optically thin the γ-rays emerge and a pair dominated jet propagates up to distances of tens of parsecs (see, for instance, Henri & Pelletier 1991). If the jet Doppler factor is known, the observed variability timescales can be used to set the size of the γ-ray photospheres. Then, the mass of the central black hole can be inferred if an emission model is available for the inner accretion disk region (e.g. Fan et al. 1999a, Cheng et al. 1999, Romero et al. 2000).

We shall use the data for the 1993.9 burst in 3C 273 published by von Montigny et al. (1997) and the jet Doppler factor inferred for that epoch in Paper I in order to estimate the mass of the primary hole in the central engine of this quasar.

3.2. Disk emission

The X-ray field that absorbs through pair creation the γ-rays generated in the vicinity of the black hole is produced by the hot inner region of the accretion disk. The state of the plasma there depends on the strength of the thermal coupling between electrons and ions. In two temperature (2T) disks, the viscosity mainly heats ions that transfer energy to electrons by Coloumb scattering. The efficient cooling of the electrons through inverse Compton interactions with UV and optical photons from the outer parts of the disk leads to different temperatures for ions and leptons ($T_{\rm i} > T_{\rm e}$). This kind of models predicts the observed power-law X-ray spectrum and a radial variation of the intensity (Shapiro et al. 1976, Eilek & Kafatos 1983). Typical electron temperatures are $T_{\rm e} \stackrel{>}{\sim} 10^9$ K. Alternatively, models with a single temperature hot corona cooled by soft photons from an underlying cool disk can also reproduce the observed spectra (e.g. Liang 1979).

Following Becker & Kafatos (1995) we shall represent the X-ray intensity of both kind of emission disk models by:

$$I = I_0 \left(\frac{E}{m_{\rm e} c^2} \right)^{-\alpha} \left(\frac{r}{r_{\rm g}} \right)^{-\xi}, \tag{11}$$

where $\xi = 0$ corresponds to a single temperature model and $\xi = 3$ to a 2T-disk. The X-ray emitting region extends from the inner disk radius $r_{\rm in}$ to a radius $r_{\rm o}$. The exact value of this latter radius is not well known due to the uncertainties in the viscosity parameter, but typically it should lay between $30r_{\rm g}$ and $100r_{\rm g}$.

3.3. Opacity to γ-ray propagation

The optical depth to pair creation for a γ-ray of energy E created at a height z above the center of the unperturbed disk (small

deviations due to precession do not significantly change the results) and propagating outward along the z-axis is:

$$\tau_{\gamma\gamma}(E, z) = \int_z^\infty \alpha_{\gamma\gamma}(E, z_*) \, dz_*, \tag{12}$$

where $\alpha_{\gamma\gamma}$ is the photon-photon absorption coefficient. Becker & Kafatos (1995) have calculated this coefficient for propagation along the disk axis using the X-ray disk intensity given by Eq. (11) with the result:

$$\alpha_{\gamma\gamma} \approx A \left(\frac{z}{r_{\rm g}} \right)^{-2\alpha-4} \left(\frac{E}{4m_{\rm e}c^2} \right)^\alpha, \tag{13}$$

where

$$A = \frac{\pi I_0 \sigma_{\rm T} \Psi(\alpha)}{(2\alpha + 4 - \xi)c} \left[\left(\frac{r_{\rm o}}{r_{\rm g}} \right)^{2\alpha+4-\xi} - \left(\frac{r_{\rm in}}{r_{\rm g}} \right)^{2\alpha+4-\xi} \right]. \tag{14}$$

Here, $\sigma_{\rm T}$ is the Thomson cross section, the function $\Psi(\alpha)$ is plotted in Fig. 1 of Becker & Kafatos' paper, and the intensity I_0 can be estimated from the observed X-ray flux, $F_{\rm KeV}$, by Eq. (5.1) of the same paper.

If the height over the disk where the radiation field becomes transparent to γ-rays of a given energy is known from variability observations, then the condition

$$\tau_{\gamma\gamma} \sim 1 \tag{15}$$

can be used to obtain the black hole mass. EGRET observations imposes a constraint to the size of the γ-spheres at $E > 100$ MeV given by:

$$z_\gamma \leq ct_{\rm v} \frac{\delta}{1+z} \quad \text{cm}, \tag{16}$$

where δ is the Doppler factor.

3.4. Mass estimates

We shall compute the mass of the primary black hole in 3C 273 using Eqs. (12-16). We shall consider different disk models characterized by the type of black hole (which determines $r_{\rm in}$), the X-ray emission structure given by parameter ξ in Eq. (11), and the outer radius of the X-ray emitting region. These models are specified in Table 1 and labeled from A to H.

In our calculations we shall adopt the X-ray flux $F_{\rm KeV} = 9.8$ μJy measured by ASCA simultaneously with the 1993 variations detected by EGRET (von Montigny et al. 1997). The Doppler factor for this epoch is $\delta \sim 7$ (Paper I) and the X-ray spectral index is $\alpha \sim 1.5$. Actually, since probably a significant part of the emission is originated in the relativistic jet and not in the accretion disk, we shall obtain an upper bound to the primary mass. The results of the calculations, where γ-ray photons of 1 GeV were considered, are shown in the second column of Table 2. The values are in the range $10^9 - 10^{10} \, M_\odot$. A model for a Kerr black hole with a 2T-disk whose X-ray emitting region extends up to 100 $r_{\rm g}$ yields an upper mass of $\sim 7.7 \times 10^9$ $M_\odot$.

Table 1. Models.

Model	BH Type	Disk Type	R_0 ($R_{\rm g}$)
A	Schwarzschild	$\xi = 3$	100
B	Schwarzschild	$\xi = 0$	100
C	Schwarzschild	$\xi = 3$	30
D	Schwarzschild	$\xi = 0$	30
E	Kerr	$\xi = 3$	100
F	Kerr	$\xi = 0$	100
G	Kerr	$\xi = 3$	30
H	Kerr	$\xi = 0$	30

These mass estimates are consistent with previous calculations based on different methods. Kafatos (1980) estimates a mass of $\sim 10^{10} \, M_\odot$, whereas Dermer & Gehrels (1995) notice that the minimum black hole mass implied by Eddington-limited accretion estimated from OSSE and EGRET observations in the Klein-Nishima regime is about $10^8 \, M_\odot$. By other hand, the ultraviolet excess in the spectrum can be fitted just by optically thick disk models which require masses of $\sim 5 \times 10^8 \, M_\odot$ (Malkan 1983, Kriss et al. 1999). Laor (1998) estimates a mass $\sim 10^9 \, M_\odot$ from the measured velocities of Hβ-emitting clouds. The fact that γ-ray variability in 3C 273 is not so rapid as in other γ-ray blazars also supports a particularly high mass value for the central object (Romero et al. 2000).

4. Mass of the secondary

In order to estimate the secondary mass, further constraints on $T_{\rm m}$ are required. We shall turn to the optical lightcurve in search for periodic behaviour that could provide information on the orbital period of the system.

4.1. Optical lightcurves

A secondary black hole in a non-coplanar close orbit must cross the outer, non-precessing parts of the accretion disk. These collisions should lead to periodic flares at optical wavelengths. The physics of the hole-disk interactions depends on many factors, whose influence is not well known. Letho & Valtonen (1996) discuss some aspects of the problem in connection with their binary model for OJ 287. The amplitude of the expected flares is uncertain, and in a very complex lightcurve as the one of 3C 273, where several different contributions to the overall variability are present, the detection of the periodic signals can be difficult.

Different periodicities for the lightcurve of 3C 273 have been claimed in the past. Angione & Smith (1985) presented a critical discussion of the controversial evidence. Recently, Fan et al. (2000) have investigated the possible presence of periodic signals in the entire historical (1887–1996) B-band lightcurve using two different, well-proven methods: the Jurkevich method (Jurkevich 1971, see also Fan 1999) and the discrete correlation function method (e.g. Edelson & Krolik 1988). They have found evidence for the existence of ~ 2.0, ~ 13.5, and ~ 22.5-year periods with both methods. The 2-year period is detected at a confidence level of about 10σ. The same period is also detected

when the analysis is restricted to the last 35 yr, where the data are more abundant, contrary to what happens with the 13.5-yr period.

If the 2-yr periodicity is real and the result of the disk penetration by the secondary (two per orbit), then the orbital period, corrected by redshift, would be $T_m \sim 3.4$ yr, and the orbital radius given by Kepler's law:

$$r_m^3 = \frac{G(m+M)T_m^2}{4\pi^2}. \tag{17}$$

Since the periodic signal seems to be constant (say within a $\sim 10\%$) throughout the historical lightcurve, additional constraints are introduced by the requirement that losses due to gravitational radiation do not significantly change the orbit. The timescale for these losses in a close supermassive binary is given by (e.g. Begelman et al. 1980, Shapiro & Teukolsky 1983):

$$\begin{aligned} \tau_0 &= |r/\dot{r}| \\ &\sim \frac{5}{256} \frac{c^5}{G^3} \frac{r_m^4}{(m+M)^2} \frac{1}{\mu}, \end{aligned} \tag{18}$$

where $\mu = mM/(m+M)$ is the reduced mass of the system.

The relative constancy of the period implies that $\tau_0 > 1000$ yr, which translates into a maximum possible value of the secondary black hole mass. Eq. (17) then imposes a maximum value to r_m. For calculation purposes we shall adopt $\tau_0 = 1000$ yr in order to obtain upper limits to the different model parameters.

4.2. Results

The results of our calculations for the different models defined in Table 1 are given in Table 2, where, from left to right we list the model code, the upper limit to the mass of the primary, the maximum mass of the secondary, and the corresponding maximum orbital radius. The radius r_d of the precessing part of the disk is unknown, but it is constrained by the requirement of not exceeding the size for which efficient communication at the sound speed fails, because otherwise the disk would not precess as a near-rigid body. The sound speed in the inner regions of the disk is $c_s \overset{>}{\sim} \Omega_p r_d$.

Additionally, Eq. (10) is valid only as far as r_m is significantly larger than r_d. In models where both black hole masses are similar, r_d results of the same order of r_m. In particular, our family of models for 3C 273 satisfies

$$\frac{r_d}{r_m} \approx 0.5 \left(\frac{M}{m}\right)^{2/3}. \tag{19}$$

The models presented, then, provide a correct representation of the physical situation when $m > M$. Otherwise, the approximations on which our semi-analytical treatment is based are no longer valid. A quite tenable model, for instance, occurs when r_d is one order of magnitude smaller than r_m, which implies that $m = 10M$. The lifetime of a model with masses $m = 5 \times 10^9$ and $M = 5 \times 10^8$ $M_\odot$ is about 5.7×10^4 yr, and the corresponding precessing disk has a radius $r_d \sim 4 \times 10^{15}$ cm.

Table 2. Results for different models (upper limits).

Model	M ($10^8 M_\odot$)	m ($10^8 M_\odot$)	r_m (10^{16} cm)
A	55.93	32.34	7.05
B	31.96	56.67	7.06
C	143.41	15.34	8.58
D	105.78	19.20	7.92
E	76.95	24.63	7.39
F	31.98	56.62	7.06
G	202.36	12.01	9.48
H	106.58	19.09	7.94

The possible values of the secondary masses in the present family of models are larger than those found for the secondary in OJ 287 (Lehto & Valtonen 1996, Valtonen & Lehto 1997). In Valtonen & Lehto's model, however, there is just one disk penetration per orbit and the precession of the disk is not considered. Katz (1997) also studied OJ 287 from a similar approach to the one used in this paper, but he did not compute detailed models because of the lack of bounds for the many free parameters. He only suggested that the primary would be constrained to masses $< 2.4 \times 10^9$ $M_\odot$ under some reasonable assumptions.

4.3. Longer periodicities

The possible presence of periodicities of ~ 13.5 and ~ 22.5 yr in the optical lightcurve (also suggested by Babadzhayants & Belokon' 1993) might be due to thermal instabilities triggered by the external perturbations in the accretion disk. The behaviour of a thermally unstable disk depends on the prescription for the viscosity parameter α_{visc}. If α_{visc} is constant, at least over relatively large disk regions, the instabilities cannot propagate too far and relatively rapid variability can be produced (timescales of $\sim$ tens of years for supermassive holes). On the contrary, varying α_{visc} prescriptions allow that more extended regions of the disk be affected by the instabilities, leading to large-scale global luminosity changes over timescales of millions of years (e.g. Mineshige & Shields 1990).

For slim disks with constant viscosity parameter, the timescales of the local thermal instabilities is (Wallinder et al. 1992):

$$\tau \sim 3.2 \times 10^{-4} \alpha_{visc}^{-1} [x^{1/2}(x-1)M_8] \quad \text{yr}, \tag{20}$$

where $x = r/r_g$ is the radius at which the instability occurs and M_8 is the accreting black hole mass in units of 10^8 $M_\odot$. If we assume that the instabilities arise at $r = r_d$, where the precession perturbs the disk structure, then a value $\alpha_{visc} = 0.05$ predicts a timescale of ~ 13.5 yr for the model mentioned in Sect. 5.2 (i.e $M_8 = 5$ and $r = r_d = 4 \times 10^{15}$ cm). Similarly, instabilities in the outer disk triggered by the disk penetration could produce quasi-periodic optical signals with larger timescales (e.g. 22.5 yr) if α_{visc} has larger values in the outer regions.

4.4. Superluminal components

The passage of the secondary black hole through the accretion disk every two years (in the observer's frame) could produce, besides variations in the optical emission, a density wave which propagates at the local sound velocity from the radius r_m towards the central black hole. This perturbation should change the accretion rate and consequently the amount of material injected into the relativistic jets, originating a shock wave which would be observed as a superluminal feature through VLBI at radio frequencies. In fact, the strongest superluminal components in 3C 273 seem to occur with such periodicity (Abraham et al. 1996). Considering that the sound velocity is close to c in the innermost region of the disk, we should expect, from the parameters given in Table 2, a delay of at least a month between the optical flare and the formation of a new shock in the relativistic jet. Abraham & Botti (1990) analyzed the lightcurves of this quasar at the V band, 22 GHz, and 43 GHz, for the epoch between 1984 and 1989, and found a correlation coefficient of 0.71 and a delay of 8 months between peaks in the V-band and the 22-GHz lightcurves. Taking into account the time at which the superluminal features were optically thick at radio wavelengths and using VLBI data to identify the formation epoch for the features, we find that component C9 in Abraham et al. (1996) was formed towards 1988.4, while an optical-infrared flare occurred at 1988.17 (Courvoisier et al. 1988). It is important to remark, however, that an exact periodicity in the appearance of superluminal features should not be expected, for several reasons. First, the jet precession changes the timescales in the observer's reference frame. Second, the time delay between the crossing of the disk by the secondary and the formation of the shock in the jets can vary if the density wave is fragmented (e.g. due to local turbulence) or there are drastic changes in the sound speed. Finally, other perturbations (arisen, for instance, from orbiting stars) can generate changes in the accretion rate and lead to shock formation. Jet interactions with clouds (discussed in Paper I), also could result in the formation of strong shocks moving down the relativistic flow.

5. Gravitational radiation

In a close massive black hole binary, gravitational radiation shrinks the orbit on a timescale given by Eq. (18). The gravitational luminosity when the binary radius is r_m results (e.g. Shapiro & Teukolsky 1983):

$$L_0 = \frac{32}{5}\mu^2 \frac{(m+M)^3}{r_m^5}\frac{G^4}{c^5}. \tag{21}$$

In Table 3 we list the upper limit to the current gravitational luminosity of the binary in the different models considered for 3C 273.

At the end of its evolution, the binary system merges producing an intense burst of gravitational waves (Thorne & Braginsky 1976, Fukushige et al. 1992). The period of the emerging wave is given by:

$$P_{burst} \approx \frac{3\sqrt{3}\pi\epsilon(m+M)}{c^3}(1+z), \tag{22}$$

Table 3. Gravitational losses and gravitational wave bursts.

Model	L_0 (10^{50} erg s^{-1})	P_{burst} (10^6 s)	F_{burst} (erg s^{-1} cm^{-2})	$\langle h \rangle$ (10^{-12})
A	2.68	0.82	~ 14	0.76
B	2.68	0.82	~ 14	0.76
C	2.68	1.47	~ 14	1.38
D	2.68	1.16	~ 14	1.08
E	2.68	0.94	~ 14	0.88
F	2.68	0.83	~ 14	0.77
G	2.68	1.99	~ 14	1.86
H	2.68	1.16	~ 14	1.09

where $\epsilon \sim 0.05$ is the efficiency of the gravitational energy release. The expected gravitational flux at the Earth is then:

$$F_{burst} = \frac{\epsilon(m+M)c^2}{4\pi D^2 P_{burst}(1+z)}, \tag{23}$$

where D is the luminosity distance. The gravitational wave burst will have a polarization-average dimensionless amplitude (Thorne & Braginsky 1976) of:

$$\langle h \rangle \approx \left(\frac{8\pi G F_{burst} P_{burst}^2}{c^3} \right)^{1/2}. \tag{24}$$

In Table 3 we also provide upper limits of all these characteristic parameters for the final supermassive merger in 3C 273 within each model. Although remote in the future, the burst characteristics might be similar within the order of magnitude to events of the same kind that could be occurring in other quasars and active galaxies. Fukushige at al. (1992) estimate that such episodes could be as frequent as 0.5 per year. Both LIGO/VIRGO and LISA gravitational detectors will be ineffective for waves of such amplitudes (e.g. Thorne 1998), but their detection could be made through Doppler tracking of interplanetary spacecrafts as originally suggested by Thorne & Braginsky (1976).

6. Pair annihilation radiation

One of the most interesting predictions of the precessing jet model for 3C 273 is that, if, as it was suggested by several authors (e.g. Wardle et al. 1998), the matter content of the jet is formed by electron–positron pairs, then the blueshifted annihilation line should display an oscillation in the spectrum originated in the varying Doppler factor. Such a possibility was briefly commented in Paper I.

The intensity of the annihilation line will depend on the initial jet density. The expected luminosity from electron–positron annihilations is (e.g. Henri et al. 1993):

$$L_{\gamma,\,obs}^{ann} = \delta^4 L_{\gamma,\,jet}^{ann} \tag{25}$$

with

$$L_{\gamma,\,jet}^{ann} = \int (E_+ + E_-)R_\pm f(E_-)f(E_+)dE_+dE_-dV \tag{26}$$

Here, $R_\pm$ is the pair annihilation rate (e.g. Coppi & Blandford 1990) and $f_\pm(E_\pm)$ is the energy distribution of the pairs, assumed here to be a power law of index p. In the conditions of the inner jet, the annihilation radiation will dominate the inverse Compton radiation for pair densities $n_\pm \gtrsim 10^9$ cm^{-3} (Böttcher & Schlickeiser 1996). For such a minimum density, a jet radius of ~ 10 gravitational radii, and a typical length scale of $\sim 3.6 \times 10^{16}$ cm (Roland & Hermsen 1995), we get:

$$L_\gamma^{\mathrm{ann}}{}_{\mathrm{jet}} = 5.4 \times 10^{46} \quad \mathrm{erg\ s^{-1}}, \tag{27}$$

where we have considered a central black hole mass corresponding to model E in Table 2.

In the observer's frame, using the Doppler factor expected for year 2001 in Abraham & Romero's model ($\delta \sim 3$), the luminosity results:

$$L_{\gamma,\mathrm{obs}}^{\mathrm{ann}} = 4.3 \times 10^{48} \quad \mathrm{erg\ s^{-1}}. \tag{28}$$

At a redshift $z = 0.158$, this yields a flux on Earth at 1 MeV of

$$F_\gamma^{\mathrm{ann}} \sim 10^{-2} \quad \mathrm{ph\ s^{-1}\ cm^{-2}}. \tag{29}$$

This value is well above the sensitivity limit of the spectrometer SPI to be launched with the INTEGRAL mission in 2001, in such a way that if the jet is pair dominated the blue-shifted annihilation line should be detected.

The detection of the electron-positron annihilation line in 3C 273 would be an important result by itself with many additional payoffs. In particular,

- The exact blue-shifting of the line can be used to impose strong constraints to the actual value of H_0 according to Abraham & Romero's model.
- The intensity of the line can be used to compute the actual density of electron-positron pairs in the source. This is important to constrain models of jet formation.
- If the observations might be extended up to year 2006, when the jet precession enters in a rapid change phase in the observer's frame, they could reveal fine details of the precession mechanism, as for instance the existence of a rapid nodding as observed in stellar-size systems like SS433.
- Repeated observations in the first two years of operation of the SPI instrument could show intensity fluctuations that might be due to shock compression of the flow as predicted by Romero (1996). Simultaneous Earth-based optical and radio variability observations in the continuum could be used to probe the innermost structure of the jet.

7. Conclusions

We have presented a binary black hole model for the central engine of 3C 273. The precession of the inner jet results from the tidal perturbation of the accretion disk produced by the secondary hole, which moves in a non-coplanar orbit. We have estimated the upper masses of the black holes as well as other system parameters within a variety of models, including both Schwarzschild and Kerr geometries for the central hole and different types of accretion disks. Estimates of current and future gravitational losses have been presented.

Our model provides a dynamic justification of the purely kinematic interpretation of the VLBI superluminal behaviour of 3C 273 presented by Abraham & Romero (1999). Future space missions as the European INTEGRAL observatory will be able to test some of the predictions of this model and will contribute to increase our understanding of one of the most interesting and studied quasars.

References

Abraham Z., Botti L.C., 1990, In: Zensus J.A., Pearson T.J. (eds.) Parsec-Scale Radio Jets. Cambridge University Press, Cambridge, p. 226
Abraham Z., Carrara E.A., Zensus J.A., et al., 1996, A&AS 115, 543
Abraham Z., Romero G.E., 1999, A&A 344, 61 (Paper I)
Angione R.L., Smith H.J., 1985, AJ 90, 2474
Babadzhayants M.K., Belokon' E.T., 1993, Astron. Rep. 37, 127
Becker P.A., Kafatos M., 1995, ApJ 453, 83
Begelman M.C., Blandford R.D., Rees M.J., 1980, Nat 287, 307
Bignami G.F., Bennett K., Buccheri R., et al., 1981, A&A 93, 71
Biretta J.A., Cohen M.J., Hardebeck H.E., et al., 1985, ApJ 292, L5
Blandford R.D., Levinson A., 1995, ApJ 441, 79
Böttcher M., Schlickeiser R., 1996, A&AS 120, 575
Cheng K.S., Fan J.H., Zhang L., 1999, A&A 352, 32
Cohen M.H., Cannon W., Purcell G.H., et al., 1971, ApJ 170, 207
Cohen M.H., Zensus J.A., Biretta J.A., et al., 1987, ApJ 315, L89
Coppi P.S., Blandford R.D., 1990, MNRAS 245, 453
Courvoisier T.J-L., Robson E.I., Blecha A., et al. 1988, Nat 335, 330
Dermer C.D., Gehrels N., 1995, ApJ 447, 103
Edelson R.A., Krolik J.H., 1988, ApJ 333, 646
Eilek J.A., Kafatos M., 1983, ApJ 271, 804
Fan J.H., 1999, MNRAS 308, 1032
Fan J.H., Xie G.Z., Bacon R., 1999a, A&AS 136, 13
Fan J.H., Romero G.E., Lin R.G., 2000, Acta Astron. Sin. in press
Fukushige T., Ebisuzaki T., Makino J., 1992, ApJ 396, L61
Gaskell M., 1996, ApJ 464, L107
Henri G., Pelletier G., 1991, ApJ 383, L7
Henri G., Pelletier G., Roland J., 1993, ApJ 404, L41
Jurkevich I., 1971, Ap&SS 13, 154
Kaastra J.S., Roos N., 1992, A&A 254, 96
Kafatos M., 1980, ApJ 236, 99
Katz J.I., 1973, Nature Phys. Sci. 246, 87
Katz J.I., 1980, ApJ 236, L127
Katz J.I., 1997, ApJ 478, 527
Katz J.I., Anderson S.F., Grandi S.A., et al., 1982, ApJ 260, 780
Krichbaum T.P., Booth R.S., Kus A.J., et al., 1990, A&A 237, 3
Kriss G.A., Davidsen A.F., Zheng W., et al., 1999, ApJ 527, 683
Laor A., 1998, ApJ 505, L83
Larwood J.D., 1997, MNRAS 290, 490
Larwood J.D., 1998, MNRAS 299, L32
Larwood J.D., Nelson R.P., Papaloizou J.C.B., et al., 1996, MNRAS 282, 597

Lehto H.J., Valtonen M.J., 1996, ApJ 460, 207
Liang E.P.T., 1979, ApJ 231, L111
Lichti G.G., Balonek T., Courvoisier T.J-L., et al., 1995, A&A 298, 711
Malkan M.A., 1983, ApJ 268, 582
Mineshige S., Shields G.A., 1990, ApJ 351, 47
Papaloizou J.C.B., Terquem C., 1995, MNRAS 274, 987
Papaloizou J.C.B., Terquem C., Lin D.N.C., 1998, ApJ 497, 212
Roland J., Hermsen W., 1995, A&A 297, L9
Romero G.E., 1996, A&A 313, 759
Romero G.E., Combi J.A., Cellone S.A., 2000, In: McConnell M.L., Ryan J.M. (eds.), Proceedings of the Fifth Compton Symposium, AIP, NY, p. 333
Roos N., 1981, A&A 104, 218
Roos N., 1988, ApJ 334, 95
Roos N., Kaastra J.S., Hummel C.A., 1993, ApJ 409, 130
Sakimoto P.J., Coroniti F.V., 1981, ApJ 247, 19
Schmidt M., 1963, Nat 197, 1040
Shapiro S.L., Lightman A.P., Eardley D.M., 1976, ApJ 204, 187
Shapiro S.L., Teukolsky S.A., 1983, In: Black Holes, White Dwarfs, and Neutron Stars. John Wiley & Sons, NY, p. 476

Sillampää A., Haarala S., Valtonen M.J., et al., 1988, ApJ 325, 628
Swanenburg B.N., Bennett K., Bignami G.F., et al., 1978, Nat 275, 298
Terquem C., Eislöffel J., Papaloizou J.C.B., et al., 1999, ApJ 512, L131
Thorne K.S., Braginsky V.B., 1976, ApJ 204, L1
Thorne K.S. 1998, In: Wald R.M. (ed.) Black Holes and Relativistic Stars. The University of Chicago Press, Chicago, p. 41
Unwin S.C., Cohen M.H., Biretta J.A., et al., 1985, ApJ 289, 109
Valtaoja L., Valtonen M.J., Byrd G.G., 1989, ApJ 343, 47
Valtonen M.J., Lehto H.J., 1997, ApJ 481, L5
Villata M., Raiteri C.M., Sillampää A., et al., 1998, MNRAS 293, L13
von Montigny C., Bertsch D.L., Fichtel C.E., et al., 1993, A&AS 97, 101
von Montigny C., Aller H., Aller M., et al., 1997, ApJ 483, 161
Wallinder F.H., Kato S., Abramowicz M.A., 1992, A&AR 4, 79
Wardle J.F.C., Homan D.C., Ojha R., et al., 1998, Nat 395, 457
Wijers R.A.M.J., Pringle J.E., 1999, MNRAS 308, 207
Zensus J.A., Bääth L.B., Cohen M.H., 1988, Nat 334, 410
Zensus J.A., Unwin S.C., Cohen M.H., et al., 1990, AJ 100, 1777